ACS APPLIED MATERIALS & INTERFACES

www.acsami.org

Research Article

Cationic Covalent Organic Framework as an Ion Exchange Material for Efficient Adsorptive Separation of Biomolecules

Imann Mosleh, Ahmad R. Khosropour, Hazim Aljewari, Christina Carbrello, Xianghong Qian, Ranil Wickramasinghe, Alireza Abbaspourrad, and Robert Beitle*

Cite This: ACS Appl. Mater. Interfaces 2021, 13, 35019−35025

Read Online

ACCESS | Metrics & More | Article Recommendations | Supporting Information

ABSTRACT: Although covalent organic frameworks (COFs) have earned significant interest in separation applications, the use of COFs in biomolecule separation remains unexplored. We examined the ionic COF Py-BPy^{2+}−COF as an ion exchange material for biomolecule separation. After characterizing the properties of the synthesized COF with a variety of techniques, binding experiments with both large and small biomolecules were performed. High adsorption capacities of amino acids with different hydrophobicity and charge, as well as proteins of different isoelectric points and molecular weights, were determined in batch equilibrium experiments. Desorption experiments with mixtures of model proteins demonstrated an ability to successfully separate one protein from another with the selectivity hypothesized to be a combination of the isoelectric point, hydrophobicity, and ability to penetrate the crystalline material. Overall, the results demonstrated that Py-BPy^{2+}−COF can be exploited as a robust crystalline anion exchange biomolecule separation material.

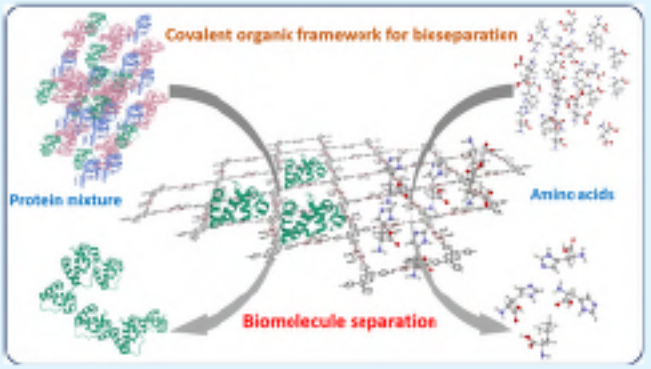

KEYWORDS: *covalent organic framework, bioseparation, ion exchange chromatography, proteins, amino acids*

1. INTRODUCTION

Bioseparation of proteins and enzymes is of high practical and theoretical importance for biotechnological, biopharmaceutical, and genetic engineering applications.[1,2] Many efforts have been devoted to different conventional techniques such as precipitation, chromatography, crystallization, and centrifugation, and more recently, membrane-based methods have been adopted for purification and separation of biomolecules.[3] Desired traits of adsorption-based media include high capacity (milligram bound per milligram sorbent), selectivity (milligram target bound/total milligram bound), and reuse potential. High-capacity separation methods such as ion exchange chromatography (IEC) are ubiquitous for the aforementioned reasons in addition to the high surface area per unit volume ratio.[4,5] IEC is known as a powerful method for the reliable separation of proteins and enzymes of interest and is based on the coordination reaction between accessible amino acids on the surface of a biomolecule and charged complexes bound to a stationary phase.[4,6] This technique has been widely exploited due to its high binding capacity, robustness, low cost, good universality, and applicability for large-scale industrial purification.[7−9] However, the dead-end porous structure, complicated pretreatment, and long separation time due to the amorphous structure can restrict its biomolecule purification efficiencies.[10] To minimize some of these drawbacks and enhance the adsorption capacity of adsorbents, engineered uniform porous materials with increased surface areas are highly desired.

Covalent organic frameworks (COFs) are porous crystalline materials with high physicochemical stability.[11] These properties have made them suitable candidates for a wide variety of applications such as gas storage and separation, catalysis, drug delivery, chemical sensing, and energy storage.[12−17] Moreover, by changing the precursors, substituents, and post-synthesis treatment, COFs with different properties and functionalities can be constructed. A major consideration while synthesizing a COF is the neutral or hydrophobic architecture needed to build the material, layer by layer, through pi stacking. Too much hydrophobicity would limit the strength of non-covalent interactions with targeted molecules.[18,19] Alternately, COFs that incorporate ionic building blocks would permit charge-based interactions for the development of functional COF bioseparation media. Ionic COFs have been previously used

Received: June 16, 2021
Accepted: July 5, 2021
Published: July 15, 2021

https://doi.org/10.1021/acsami.1c11270
ACS Appl. Mater. Interfaces 2021, 13, 35019−35025

Scheme 1. Adsorption strategies of COFs toward biomolecules: (a) adsorption of low-molecular-weight biomolecules (amino acids) and (b) adsorption of larger biomolecules (proteins)

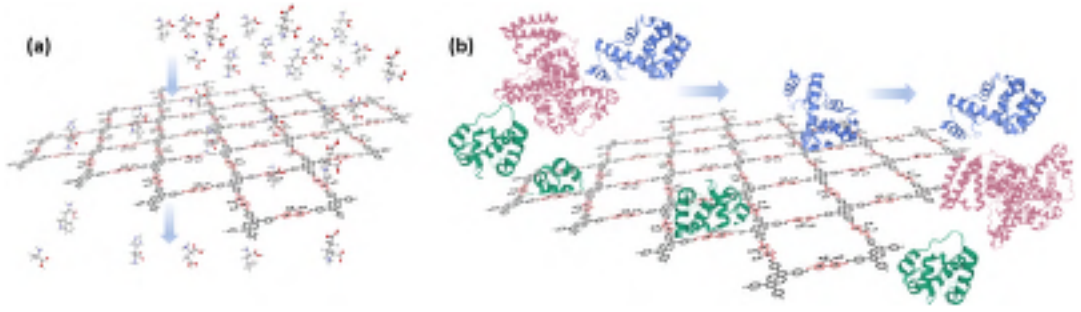

for dye pollutant removal, energy storage, and photothermal conversion.[20−22] However, to the best of our knowledge, the use of ionic COFs as ion exchange materials for biomolecule separation has not been extensively studied.

Recently, frameworks with metals as part of their architecture have been reported for protein separation.[23−26] Despite their capability in protein adsorption, both the lower stability and the possibility of metal leaching have made metal-free organic frameworks preferable for adsorption purposes. In addition, traditional ion exchange media have adsorptive groups bound to the heterogeneous material such as Sepharose, which is a cross-linked polysaccharide displaying different binding properties due to polydispersity and distribution of functional groups on the structure. The high crystallinity and stability of COFs will provide well-patterned adsorption sites on a surface with similar properties. Herein, we synthesized a neutral 2,2′-bipyridine-based COF and through chemical modification built a positively charged COF to examine as an IEC medium. Two different strategies were envisioned for adsorption. As shown in Scheme 1a, channels within the COF permits adsorption of low-molecular-weight materials within the porous network, while large-biomolecule adsorption was hypothesized to be primarily a surface event with the caveat that larger molecules could "dip" into or partially penetrate the material (Scheme 1b).

The cationic bipyridine-based COF was characterized, and ultimately, its adsorption properties were investigated using a set of six amino acids as well as three different proteins.

2. EXPERIMENTAL SECTION

2.1. Synthesis of Py-BPy^{2+}−COF. A method adapted from Mi *et al.* was followed for cationic COF (Py-BPy^{2+}−COF) synthesis.[22] Briefly, the 2,2′-BPy-DCA monomer (0.04 mmol, 8.5 mg) and Py-TA linker (0.02 mmol, 11.3 mg) were mixed in mesitylene/dioxane/6 M HOAc (5/5/1 by vol.; 1.1 mL) inside a 10 mL Pyrex tube. After five cycles of freeze−pump−thaw treatment, the reaction proceeded at 120 °C for 6 days in an oven. The neutral Py-BPy−COF was obtained after filtration, DI water triple wash, and vacuum-drying overnight at 60 °C. The neutral Py-BPy−COF was then mixed with 1,2-dibromoethane (1:4 molar ratio of Py-BPy−COF/1,2-dibromoethane) in nitrobenzene and refluxed overnight. Consequently, the cationic Py-BPy^{2+}−COF was obtained after filtration, acetone wash, and vacuum-drying overnight at 60 °C in the form of an orange powder.

2.2. Biomolecule Adsorption. A group of six amino acids and three proteins were selected as model biomolecules for capture and release experiments. To evaluate the isothermal adsorption performance of Py-BPy^{2+}−COF, biomolecule aqueous solutions in 20 mM sodium phosphate buffer at different concentrations ranging from 0.0 to 3.0 mg mL^{-1} were ultrasonically mixed with Py-BPy^{2+}−COF (0.1 mg) at room temperature for 5 min. The concentrations of amino acids (at 210 nm) and proteins (at 280 nm) were analyzed using UV−vis spectroscopy after Py-BPy^{2+}−COF separation *via* centrifugation. Based on the following equation, the adsorption capacity at each interval was determined

$$Q = \frac{(C_0 - C)V}{m} \quad (1)$$

where Q (μg mg^{-1}) is the adsorption capacity, C_0 (μg mL^{-1}) is the initial protein concentration, C (μg mL^{-1}) is the residual protein concentration in the supernatant, V (mL) is the volume of the initial solution, and m (mg) is the amount of Py-BPy^{2+}−COF.

2.3. Protein and Amino Acid Desorption of Py-BPy^{2+}−COF. To characterize protein desorption, Py-BPy^{2+}−COF was first treated with different proteins at 2.0 mg mL^{-1} concentration. After solid recovery through centrifugation, the treated Py-BPy^{2+}−COF samples were incubated with 200 μL of 2 M NaCl solution for 5 min. The mixtures were centrifuged at 5000 rpm, and the supernatants were subjected to trichloroacetic acid (TCA)/acetone precipitation. Briefly, 20 μL of the TCA solution was added to 200 μL of the treated supernatants and vortexed for 10 s. The solutions were centrifuged for 3 min, and 200 μL of ice-cold acetone was added to the decanted supernatants. The precipitates were then air-dried for 3 min and dissolved in 10 μL of 8 M urea. The solutions were mixed with 15 μL of protein loading dye and heated for 4 min at 95 °C to denature the protein. The presence of protein in the mixtures was visualized using 15% polyacrylamide SDS−PAGE. After loading the solution to the gel, the samples were resolved for 40 min at 180 V. Ultimately, the gels were stained by Coomassie blue protein for 10 min and destained overnight.

The biomolecule quantification was performed using high-performance liquid chromatography (HPLC) using a 1260 Infinity HPLC instrument (Agilent Technologies, Santa Clara, CA) operated in the reverse phase mode. A Luna C18 column from Phenomenex, 5 μm, size 250 × 4.6 mm (Torrance, CA), was employed as the stationary phase. For the mobile phase, DI water and acetonitrile at a flow rate of 1 mL/min, with A8 linear gradient varying from 25 to 70% acetonitrile, were used. A diode array detector for UV absorbance was used for detection with a 5 ppb limit of detection at wavelengths of 280 and 210 nm for protein and amino acid, respectively.

2.4. Characterization. A transmission electron microscope, JEOL-1011 (JEOL-USA, Peabody, MA), was applied for structure and morphology analysis of synthesized COFs. Powder X-ray diffraction (PXRD) patterns were determined using a Bruker D8 ADVANCE ECO powder diffractometer operated at 40 kV and 25 mA. Fourier transform infrared (FT-IR) analysis of COFs was performed and FT-IR spectra were recorded on a Nicolet 6700 (Thermofisher, USA) FT-IR spectrometer. X-ray photoelectron spectroscopy (XPS) measurements were analyzed using a VersaProbe station (Physical Electronics, Chanhassen, MN) with a monochromatic Al Kα beam. The biomolecule adsorption measurement was carried out using a Beckman Coulter DU 800 UV−Vis spectrophotometer (Beckman Coulter, Brea, CA).

https://doi.org/10.1021/acsami.1c11270
ACS Appl. Mater. Interfaces 2021, 13, 35019−35025

Scheme 2. Schematic illustration of Py-BPy^{2+}–COF synthesis: (a) synthesis of Py-BPy–COF and (b) transformation of Py-BPy–COF to the cationic Py-BPy^{2+}–COF

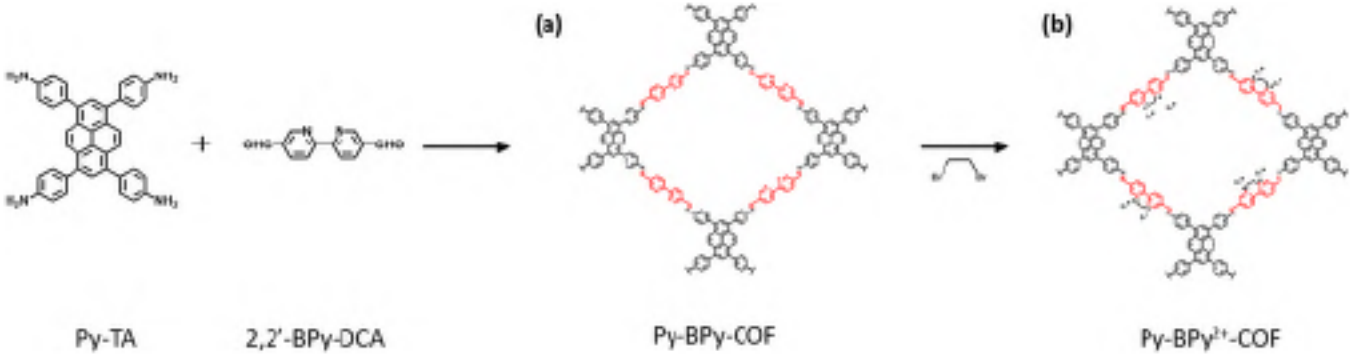

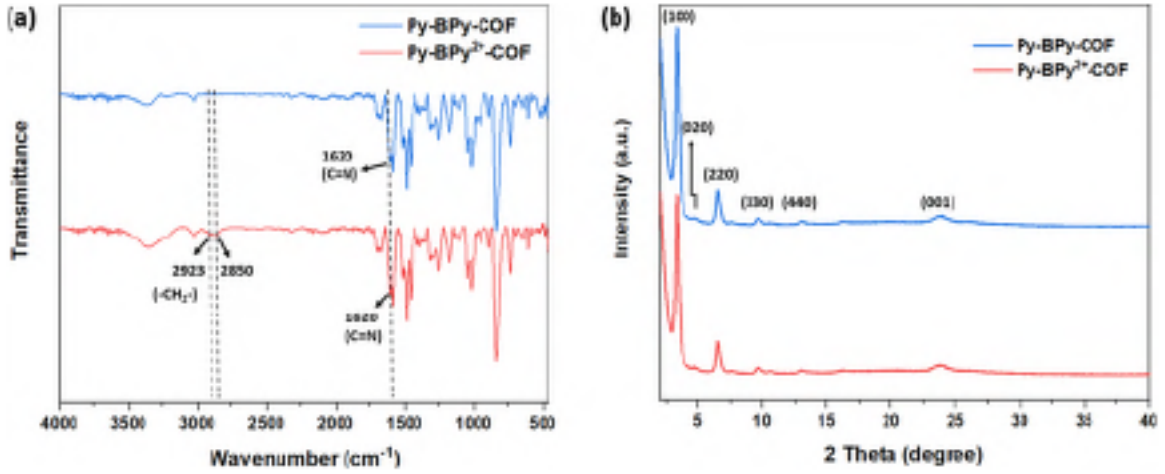

Figure 1. (a) FT-IR spectra of COFs. The appearance of methylene (–CH_2–) indicated the successful treatment of Py-BPy–COF with 1,2-dibromoethane to obtain Py-BPy^{2+}–COF. (b) PXRD patterns of COFs.

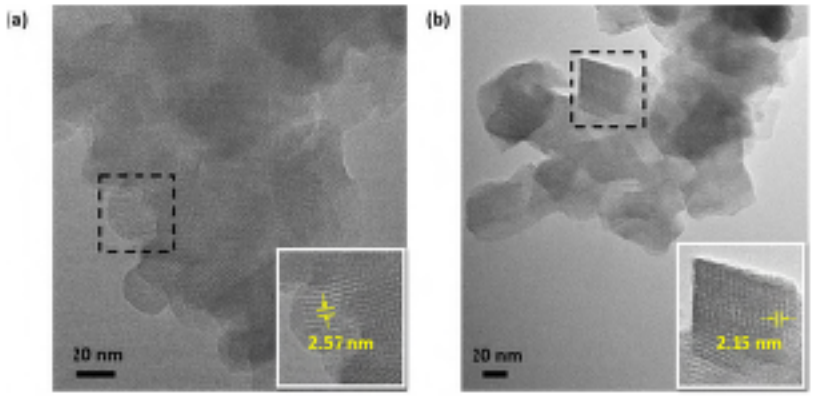

Figure 2. TEM characterization of (a) Py-BPy–COF and (b) Py-BPy^{2+}–COF.

3. RESULTS AND DISCUSSION

3.1. Preparation and Characterization of Py-BPy^{2+}–COF. Py-BPy–COF was synthesized by the solvothermal reaction of Py-TA and 2,2′-BPy-DCA in dioxane and mesitylene in the presence of acetic acid (Scheme 2a).[22,27] The yellow Py-BPy–COF was then mixed with 1,2-dibromoethane and refluxed in nitrobenzene. Microcrystalline Py-BPy^{2+}–COF was obtained in a 75% yield in the form of an orange solid (Scheme 2b).[22]

To validate the success of synthesis, COFs were primarily characterized by XPS, confirming the presence of nitrogen forms as well as the bromide anion. The Py-BPy^{2+}–COF nitrogen 1s peak was deconvoluted into two peaks appearing at 397 and 399 eV, assigned to the imine and diquat forms of nitrogen, respectively (Figure S1a).[22] As the nitrogen content of Py-BPy–COF was detected predominantly in the form of imines and pyridines, the detection of nitrogen at 399 eV was attributed to the high-yield transformation of pyridines to diquats in Py-BPy^{2+}–COF after treatment with 1,2-dibromoethane, in which no signal corresponding to pyridine nitrogen was detected.[22] Moreover, the Br 3d XPS spectrum showed a peak at the binding energy of around 66.4 eV, attributed to the formation of the bromide anion and cyclic alkylated diquats in

https://doi.org/10.1021/acsami.1c11270
ACS Appl. Mater. Interfaces 2021, 13, 35019−35025

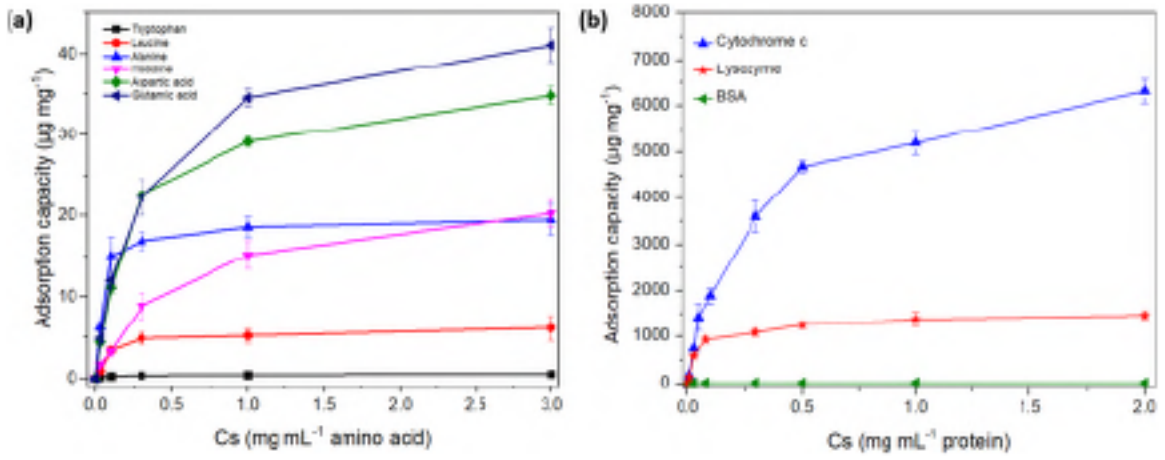

Figure 3. Adsorption capacity of Py-BPy^{2+}−COF toward (a) different amino acids and (b) different proteins.

the Py-BPy^{2+}−COF structure. The detected peak at a binding energy of around 69.2 eV corresponded to bromoalkene due to the formation of the linear alkylated diquat species (Figure S1b).

The stretches of imine (C=N) bonds were detected at 1620 cm^{-1} for both neutral and charged samples in FT-IR spectra. Meanwhile, the peaks corresponding to the stretching vibration of methylene (−CH_2−) were detected at 2923 and 2850 cm^{-1} in Py-BPy^{2+}−COF, while they were absent in the Py-BPy−COF spectrum. These signals indicated the presence of the ethylene groups attached to Py-BPy^{2+}−COF after treatment with 1,2-dibromoethane (Figure 1).

To confirm the crystallinity of structures, PXRD analysis was carried out (Figure 1b). The PXRD patterns of Py-BPy−COF exhibited main diffraction peaks at 3.16, 4.59, 6.38, 9.68, 12.94, and 23.78°, which are assigned to the (100), (020), (220), (330), (440), and (001) facets, respectively, confirming the crystalline structure of the prepared Py-BPy−COF.[27] Comparing the PXRD patterns, Py-BPy^{2+}−COF is as crystalline with the eclipsed conformation as Py-BPy−COF, indicating that the framework composition remained unchanged after the attachment of the ethylene group.

PXRD analysis was well-supported by corresponding transmission electron microscopy (TEM) images. As shown in Figure 2, periodic porous frameworks were formed, and the existence of lattice fringes confirmed the high degree of crystallinity for both COFs. The inset images depict the distinct channel sizes of 2.57 and 2.15 nm for Py-BPy−COF and Py-BPy^{2+}−COF, respectively. The formation channels with the smaller size in Py-BPy^{2+}−COF were attributed to the cyclic and linear alkylated diquats after treatment with 1,2-dibromoethane (Figure S3). These observations were consistent with pore diameter size distribution measurements obtained through simulated COF structures.[28−30]

3.2. Adsorption of Biomolecules Using Py-BPy^{2+}−COF. For the adsorption capacity evaluation of Py-BPy^{2+}−COF, the binding capacities of different amino acids (tryptophan, leucine, alanine, histidine, aspartic acid, and glutamic acid) as well as three model proteins [cytochrome c, lysozyme, and bovine serum albumin (BSA)] were investigated. The binding ability of Py-BPy^{2+}−COF was primarily explored for amino acids of different hydrophobicities in a pH 7.8 buffer. We hypothesized that the adsorption of low-molecular-weight biomolecules takes place within the porous network (Scheme 1a). Moreover, Py-BPy^{2+}−COF represents an anion exchange material, and since it is positively charged, the pH of separation experiments was greater than the isoelectric point (pI) (Table S1). As shown in Figure 3a, the binding curves demonstrate saturation (type I) curves indicative of Langmuir-style adsorption. Different saturation capacities ranging from 0.46 to 41.1 μg mg^{-1} for the amino acids were observed. Importantly, the maximum adsorption capacity was obtained for amino acids with lower pI values, hydrophobicity scales, and steric hindrance where the saturation capacities for aspartic acid and glutamic acid were determined to be 34.8 and 41.1 μg mg^{-1}, respectively. On the other hand, despite the lower pI values of tryptophan and leucine than that of alanine and histidine, their adsorption capacities were lower. This mixed-mode behavior indicated that saturation can be attributed to hydrophobicity, steric hindrance, and charge−charge interaction within the porous structure of Py-BPy^{2+}−COF. It is important to note that the neutral Py-BPy−COF showed very low amino acid adsorption (Figure S4). To summarize, the adsorption capacity order of the six amino acids from the highest to the lowest was glutamic acid > aspartic acid > histidine > alanine > leucine > tryptophan.

The adsorption capacity of Py-BPy^{2+}−COF was further characterized with proteins of different sizes and molecular weights in pH 10, 12, and 7.8 buffers for cytochrome c, lysozyme, and BSA, respectively. Similar to the amino acid studies, there was minimal interaction between the negatively charged proteins and neutral Py-BPy−COF (Figure S4). The porous Py-BPy^{2+}−COF acts as an anion exchange material with the unique caveat that proteins may dip into or penetrate the structure depending on the size (Scheme 1b). The adsorption equilibrium isotherms for proteins indicated a type I behavior for lysozyme and cytochrome c up to 0.5 and 1.0 mg mL^{-1}, respectively (Figure 3b). On the other hand, the binding ability for BSA was rather poor. The saturation capacity for cytochrome c was 5800 μg mg^{-1}, while for lysozyme and BSA, maximum adsorption capacities reached 1400 and 16 μg mg^{-1}, respectively.

Obviously, Py-BPy^{2+}−COF showed higher adsorption capacity for cytochrome c than that for the other two proteins. Cytochrome c is a 12 kDa protein having 104 amino acids with a hydrodynamic radius of 1.4 nm.[31] As the pore diameter of Py-BPy^{2+}−COF was 2.2 nm, it is reasonable to assume that cytochrome c was adsorbed both on the surface and within the porous structure of the COF crystal. The lower adsorption

https://doi.org/10.1021/acsami.1c11270
ACS Appl. Mater. Interfaces 2021, 13, 35019−35025

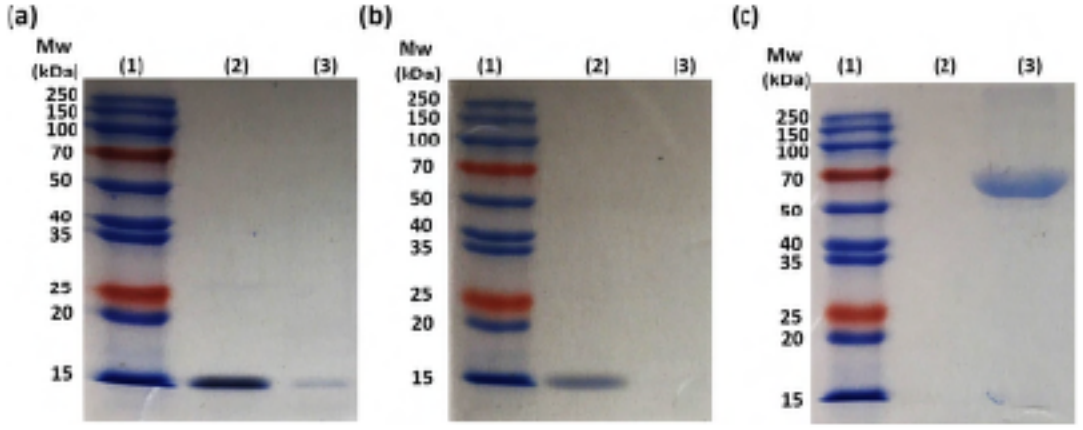

Figure 4. SDS–PAGE analysis of (a) cytochrome c, (b) lysozyme, and (c) BSA protein desorption using TCA protein precipitation. For cytochrome c and lysozyme, lane 1 represents the Mw marker, lane 2 represents protein detection prior to the treatment, and lane 3 shows desorbed proteins. For BSA, lane 1 represents the Mw marker, lane 2 depicts desorbed proteins, and lane 3 represents protein detection prior to the treatment.

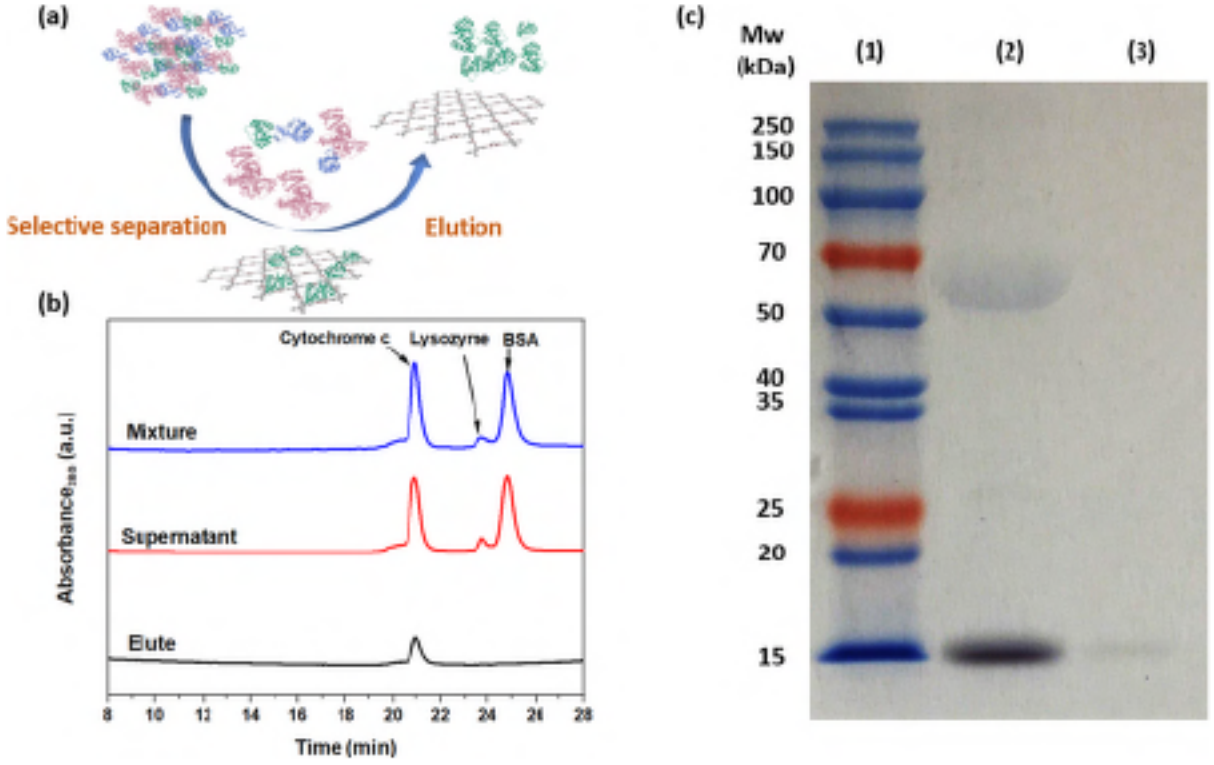

Figure 5. Selective protein separation using Py-BPy^{2+}–COF. (a) Schematic illustration of selectivity, (b) HPLC curves, and (c) SDS–PAGE analysis of protein selectivity assay.

capacity of lysozyme when compared to that of cytochrome c also supported the hypothesis of selectivity-based size and charge since the protein is slightly larger, *viz.*, a 14.3 kDa protein having 129 amino acids with a hydrodynamic radius of 1.9 nm. Finally, despite the large difference between the pI and binding buffer in the case of BSA, this last model protein was not efficiently captured. If Py-BPy^{2+}–COF acted like a common IEC material without exclusion effects, the large difference between pI and pH of the experiment would, in principle, promote binding because R-groups would be negatively charged. Significant binding was not observed and therefore could be attributed to exclusion since BSA is a 66.4 kDa protein with 607 amino acids and a hydrodynamic radius of 3.8 nm.[32,33] Any adsorption was probably a surface event and hence exhibited a lower number of bound proteins compared to cytochrome c and lysozyme. In other words, the adsorption characteristics could be explained in terms of size and charge. It is worth noting that Py-BPy^{2+}–COF demonstrates high stability in the operation range of pH (Figure S5).

3.3. Biomolecule Desorption and Selectivity of Py-BPy^{2+}–COF toward Target Proteins. After treatment with biomolecules, amino acids and proteins were eluted from Py-BPy^{2+}–COF to evaluate the desorption ability. To study the amino acid desorption of Py-BPy^{2+}–COF, glutamic acid was used as a model. Py-BPy^{2+}–COF (0.1 mg) was dispersed in a pH 7.8 buffer solution containing 3 mg mL^{-1} glutamic acid. Subsequently, the amino acid solution before being exposed to

https://doi.org/10.1021/acsami.1c11270
ACS Appl. Mater. Interfaces 2021, 13, 35019−35025

Py-BPy^{2+}−COF, the supernatant after Py-BPy^{2+}−COF treatment, and the elute were quantitatively analyzed using HPLC. Data confirmed that 1.3% of glutamic acid was adsorbed by Py-BPy^{2+}−COF (Figure S6).

As shown by SDS−PAGE analyses, major bands assigned to cytochrome c, lysozyme, and BSA were detected prior to the treatment (Figure 4). However, only a band assigned to desorbed cytochrome c was detected after the treatment, demonstrating the selectivity of Py-BPy^{2+}−COF toward cytochrome *c* (Figure 4a, lane 3).

The reusability of Py-BPy^{2+}−COF was examined for the separation of cytochrome c as a model protein in which the adsorbent remained intact and functional after at least five runs (Figure S7).

The protein selectivity assay of Py-BPy^{2+}−COF was carried out using a protein mixture containing cytochrome c, lysozyme, and BSA. After dispersing and incubating the protein mixture in a pH 10 buffer solution containing Py-BPy^{2+}−COF, the mixture of proteins, supernatant, and the elute were quantitatively analyzed using HPLC. As shown in Figure 5b, the presence of the three proteins in the mixture (blue line) was confirmed. After adsorption, 87% of cytochrome c remained in the supernatant, while the amount of other proteins essentially remained unchanged (red line). Importantly, only a single peak pertaining to cytochrome c was detected in the elute (black line), showing that 11% of the initial load of cytochrome c was captured by Py-BPy^{2+}−COF. The HPLC quantification was further confirmed by SDS−PAGE. As shown in Figure 5c, only a band indicating the selective isolation of cytochrome c was detected (lane 3), while the presence of proteins was confirmed in the protein mixture (lane 2). The excellent selective separation of cytochrome c was attributed to the positively charged nature of Py-BPy^{2+}−COF at the running pH as well as the crystalline porous structure which provided different affinity interactions. Also, the band intensity should not be construed with selectivity or capacity because of the difference in dilution between each experiment. The result confirmed the practicability and selectivity of Py-BPy^{2+}−COF toward protein adsorption in the presence of other proteins.

4. CONCLUSIONS

The use of Py-BPy^{2+}−COF in the separation of biomolecules with different hydrophobicity scales, sizes, and molecular weights was explored. Due to its crystalline porous structure, Py-BPy^{2+}−COF demonstrated the desired properties of a bioseparation medium that included high capacity and selectivity. Its structure as well as its metal-free nature makes its candidacy as an IEC medium worth the continued development.

■ ASSOCIATED CONTENT

Supporting Information

The Supporting Information is available free of charge at https://pubs.acs.org/doi/10.1021/acsami.1c11270.

Detailed experimental procedures and characterization data of compounds: NMR spectra (1H and 13C{1H}), HPLC results, and XPS spectra (PDF)

■ AUTHOR INFORMATION

Corresponding Author

Robert Beitle − *Ralph E. Martin Department of Chemical Engineering, University of Arkansas, Fayetteville, Arkansas 72701, United States;* orcid.org/0000-0001-8859-8358; Email: rbeitle@uark.edu

Authors

Imann Mosleh − *Ralph E. Martin Department of Chemical Engineering, University of Arkansas, Fayetteville, Arkansas 72701, United States; Department of Food Science, Cornell University, Ithaca, New York 14850, United States;* orcid.org/0000-0001-8763-6906

Ahmad R. Khosropour − *Department of Food Science, Cornell University, Ithaca, New York 14850, United States;* orcid.org/0000-0002-4170-0017

Hazim Aljewari − *Ralph E. Martin Department of Chemical Engineering, University of Arkansas, Fayetteville, Arkansas 72701, United States*

Christina Carbrello − *MilliporeSigma Corporation, Bedford, Massachusetts 01730, United States*

Xianghong Qian − *Department of Biomedical Engineering, University of Arkansas, Fayetteville, Arkansas 72701, United States*

Ranil Wickramasinghe − *Ralph E. Martin Department of Chemical Engineering, University of Arkansas, Fayetteville, Arkansas 72701, United States*

Alireza Abbaspourrad − *Department of Food Science, Cornell University, Ithaca, New York 14850, United States;* orcid.org/0000-0001-5617-9220

Complete contact information is available at: https://pubs.acs.org/10.1021/acsami.1c11270

Author Contributions

The manuscript was written through contributions of all authors. All authors have given approval to the final version of the manuscript.

Funding

This work was supported by the Center for Membrane Science, Engineering and Technology (MAST) and the National Science Foundation (IIP 1822101).

Notes

The authors declare no competing financial interest.

■ ACKNOWLEDGMENTS

The authors thank Tanmoy Patra for his assistance during this project.

■ REFERENCES

(1) Harrison, R. G.; Todd, P. W.; Rudge, S. R.; Petrides, D. P. *Bioseparations Science and Engineering*; Oxford University Press, 2015.

(2) Li, M.; Xiong, Y.; Qing, G. Smart Bio-Separation Materials. *Trac. Trends Anal. Chem.* 2020, *124*, 115585.

(3) Tan, S.; Saito, K.; Hearn, M. T. Stimuli-Responsive Polymeric Materials for Separation of Biomolecules. *Curr. Opin. Biotechnol.* 2018, *53*, 209−223.

(4) Briskot, T.; Hahn, T.; Huuk, T.; Hubbuch, J. Adsorption of Colloidal Proteins in Ion-Exchange Chromatography under Consideration of Charge Regulation. *J. Chromatogr. A* 2020, *1611*, 460608.

(5) Benedini, L. J.; Figueiredo, D.; Cabrera-Crespo, J.; Gonçalves, V. M.; Silva, G. G.; Campani, G.; Zangirolami, T. C.; Furlan, F. F. Modeling and Simulation of Anion Exchange Chromatography for

Purification of Proteins in Complex Mixtures. *J. Chromatogr. A* 2020, *1613*, 460685.
(6) Cummins, P. M.; Rochfort, K. D.; O'Connor, B. F. Ion-Exchange Chromatography: Basic Principles and Application. In *Protein Chromatography: Methods and Protocols*; Walls, D., Loughran, S. T., Eds.; Methods in Molecular Biology; Springer: New York, NY, 2017, pp 209−223.
(7) Janson, J.-C. *Protein Purification: Principles, High Resolution Methods, and Applications*; John Wiley & Sons, 2012.
(8) Mukherjee, R. P.; Pruchil, M. S.; Beitle, R. R.; Brune, E. M. Development of a Novel Engineered E. Coli Host Cell Line Platform with Improved Column Capacity Performance for Ion-Exchange Chromatography. *Protein Expression Purif.* 2018, *142*, 32−36.
(9) Yu, L.; Gong, L.; Bai, S.; Sun, Y. Surface DEAE Groups Facilitate Protein Transport on Polymer Chains in DEAE-Modified-and-DEAE-Dextran-Grafted Resins. *AIChE J.* 2016, *62*, 3812−3819.
(10) Großhans, S.; Wang, G.; Fischer, C.; Hubbuch, J. An Integrated Precipitation and Ion-Exchange Chromatography Process for Antibody Manufacturing: Process Development Strategy and Continuous Chromatography Exploration. *J. Chromatogr. A* 2018, *1533*, 66−76.
(11) Côté, A. P.; Benin, A. I.; Ockwig, N. W.; O'Keeffe, M.; Matzger, A. J.; Yaghi, O. M. Porous, Crystalline, Covalent Organic Frameworks. *Science* 2005, *310*, 1166−1170.
(12) Oxdemir, J.; Mosleh, I.; Abolhassani, M.; Greenlee, L. F.; Beitle, R. R.; Beyzavi, M. H. Covalent Organic Frameworks for the Capture, Fixation, or Reduction of CO2. *Front. Energy Res.* 2019, *7*, 77.
(13) Lin, S.; Diercks, C. S.; Zhang, Y.-B.; Kornienko, N.; Nichols, E. M.; Zhao, Y.; Paris, A. R.; Kim, D.; Yang, P.; Yaghi, O. M.; Chang, C. J. Covalent Organic Frameworks Comprising Cobalt Porphyrins for Catalytic CO2 Reduction in Water. *Science* 2015, *349*, 1208−1213.
(14) Wang, X.; Han, X.; Zhang, J.; Wu, X.; Liu, Y.; Cui, Y. Homochiral 2D Porous Covalent Organic Frameworks for Heterogeneous Asymmetric Catalysis. *J. Am. Chem. Soc.* 2016, *138*, 12332−12335.
(15) Bai, L.; Phua, S. Z. F.; Lim, W. Q.; Jana, A.; Luo, Z.; Tham, H. P.; Zhao, L.; Gao, Q.; Zhao, Y. Nanoscale Covalent Organic Frameworks as Smart Carriers for Drug Delivery. *Chem. Commun.* 2016, *52*, 4128−4131.
(16) Yan, D.; Wu, Y.; Kitaura, R.; Awaga, K. Salt-Assisted Pyrolysis of Covalent Organic Frameworks to Porous Heteroatom-Doped Carbons for Supercapacitive Energy Storage. *J. Mater. Chem. A* 2019, *7*, 26829−26837.
(17) Liu, H.; Li, C.; Li, H.; Ren, Y.; Chen, J.; Tang, J.; Yang, Q. Structural Engineering of Two-Dimensional Covalent Organic Frameworks for Visible-Light-Driven Organic Transformations. *ACS Appl. Mater. Interfaces* 2020, *12*, 20354−20365.
(18) Lu, Z.; Liu, Y.; Liu, X.; Lu, S.; Li, Y.; Yang, S.; Qin, Y.; Zheng, L.; Zhang, H. A Hollow Microshuttle-Shaped Capsule Covalent Organic Framework for Protein Adsorption. *J. Mater. Chem. B* 2019, *7*, 1469−1474.
(19) Lin, G.; Gao, C.; Zheng, Q.; Lei, Z.; Geng, H.; Lin, Z.; Yang, H.; Cai, Z. Room-Temperature Synthesis of Core−Shell Structured Magnetic Covalent Organic Frameworks for Efficient Enrichment of Peptides and Simultaneous Exclusion of Proteins. *Chem. Commun.* 2017, *53*, 3649−3652.
(20) Yu, S.-B.; Lyu, H.; Tian, J.; Wang, H.; Zhang, D.-W.; Liu, Y.; Li, Z.-T. A Polycationic Covalent Organic Framework: A Robust Adsorbent for Anionic Dye Pollutants. *Polym. Chem.* 2016, *7*, 3392−3397.
(21) Wang, L.; Zeng, C.; Xu, H.; Yin, P.; Chen, D.; Deng, J.; Li, M.; Zheng, N.; Gu, C.; Ma, Y. A Highly Soluble, Crystalline Covalent Organic Framework Compatible with Device Implementation. *Chem. Sci.* 2019, *10*, 1023−1028.
(22) Mi, Z.; Yang, P.; Wang, R.; Unruangsri, J.; Yang, W.; Wang, C.; Guo, J. Stable Radical Cation-Containing Covalent Organic Frameworks Exhibiting Remarkable Structure-Enhanced Photothermal Conversion. *J. Am. Chem. Soc.* 2019, *141*, 14433−14442.
(23) Ma, W.; Xu, L.; Li, X.; Shen, S.; Wu, M.; Bai, Y.; Liu, H. Cysteine-Functionalized Metal−Organic Framework: Facile Synthesis and High Efficient Enrichment of N-Linked Glycopeptides in Cell Lysate. *ACS Appl. Mater. Interfaces* 2017, *9*, 19562−19568.
(24) Shi, S.; Zhang, W.; Wu, H.; Li, Y.; Ren, X.; Li, M.; Liu, J.; Sun, J.; Yue, T.; Wang, J. In Situ Cascade Derivation toward a Hierarchical Layered Double Hydroxide Magnetic Absorbent for High-Performance Protein Separation. *ACS Sustainable Chem. Eng.* 2020, *8*, 4966−4974.
(25) Tan, S.; Long, Y.; Han, Q.; Guan, H.; Liang, Q.; Ding, M. Designed Fabrication of Polymer-Mediated MOF-Derived Magnetic Hollow Carbon Nanocages for Specific Isolation of Bovine Hemoglobin. *ACS Biomater. Sci. Eng.* 2020, *6*, 1387−1396.
(26) Wu, Y.; Sun, N.; Deng, C. Construction of Magnetic Covalent Organic Frameworks with Inherent Hydrophilicity for Efficiently Enriching Endogenous Glycopeptides in Human Saliva. *ACS Appl. Mater. Interfaces* 2020, *12*, 9814−9823.
(27) Chen, X.; Huang, N.; Gao, J.; Xu, H.; Xu, F.; Jiang, D. Towards Covalent Organic Frameworks with Predesignable and Aligned Open Docking Sites. *Chem. Commun.* 2014, *50*, 6161−6163.
(28) Hu, Y.; Dunlap, N.; Wan, S.; Lu, S.; Huang, S.; Sellinger, I.; Ortiz, M.; Jin, Y.; Lee, S.-h.; Zhang, W. Crystalline Lithium Imidazolate Covalent Organic Frameworks with High Li-Ion Conductivity. *J. Am. Chem. Soc.* 2019, *141*, 7518−7525.
(29) Bi, S.; Yang, C.; Zhang, W.; Xu, J.; Liu, L.; Wu, D.; Wang, X.; Han, Y.; Liang, Q.; Zhang, F. Two-Dimensional Semiconducting Covalent Organic Frameworks via Condensation at Arylmethyl Carbon Atoms. *Nat. Commun.* 2019, *10*, 2467.
(30) Li, S.; Liu, Y.; Li, L.; Liu, C.; Li, J.; Ashraf, S.; Li, P.; Wang, B. Enhanced Proton Conductivity of Imidazole-Doped Thiophene-Based Covalent Organic Frameworks via Subtle Hydrogen Bonding Modulation. *ACS Appl. Mater. Interfaces* 2020, *12*, 22910−22916.
(31) Akiyama, S.; Takahashi, S.; Kimura, T.; Ishimori, K.; Morishima, I.; Nishikawa, Y.; Fujisawa, T. Conformational Landscape of Cytochrome c Folding Studied by Microsecond-Resolved Small-Angle x-Ray Scattering. *Proc. Natl. Acad. Sci. U.S.A.* 2002, *99*, 1329−1334.
(32) Parmar, A. S.; Muschol, M. Hydration and Hydrodynamic Interactions of Lysozyme: Effects of Chaotropic versus Kosmotropic Ions. *Biophys. J.* 2009, *97*, 590−598.
(33) Hawe, A.; Hulse, W. L.; Jiskoot, W.; Forbes, R. T. Taylor Dispersion Analysis Compared to Dynamic Light Scattering for the Size Analysis of Therapeutic Peptides and Proteins and Their Aggregates. *Pharm. Res.* 2011, *28*, 2302−2310.

https://doi.org/10.1021/acsami.1c11270
ACS Appl. Mater. Interfaces 2021, 13, 35019−35025